Journal of Cleaner Production 452 (2024) 142122

Contents lists available at ScienceDirect

Journal of Cleaner Production

journal homepage: www.elsevier.com/locate/jclepro

Energy-efficient rapid additive manufacturing of complex geometry ceramics

Ruochen Liu [a,b], Aolin Hou [b], Prashant Dhakal [c], Chongjie Gao [c], Jingjing Qiu [e], Shiren Wang [b,c,d,*]

[a] College of Materials Science and Engineering, Beijing University of Technology, Beijing, 100124, China
[b] Department of Materials Science and Engineering, Texas A&M University, College Station, TX, 77843, USA
[c] Department of Industrial and Systems Engineering, Texas A&M University, College Station, TX, 77843, USA
[d] Department of Biomedical Engineering, Texas A&M University, College Station, TX, 77843, USA
[e] Department Mechanical Engineering, Texas A&M University, College Station, TX, 77843, USA

ARTICLE INFO

Handling Editor: Mingzhou Jin

Keywords:
Additive manufacturing
Self-sustaining reaction
Ceramic composites
Preceramic polymers
Manufacturing decarbonization

ABSTRACT

Energy-intensive industries are one of the key greenhouse gas emitters, and decarbonization of such industries is a top priority to promote global sustainability. As one of the top energy-intensive industries, ceramic manufacturing industries are urged to boost energy efficiency in ceramic structure production. In this paper, we present a rapid and low carbon footprint strategy for freeform manufacturing spatial ceramic composites. Our approach integrates layer-by-layer deposition, photothermal in-situ solidification, and self-sustaining ceramization, enabling consolidation using only 1920 J energy. Compared to state-of-the-art processes, energy consumption can be reduced by over 100-fold, resulting in an estimated 1000-fold decrease in CO_2 emissions. This energy-efficient process also demonstrates the rapid fabrication of ceramic gyroid heat exchangers, capable of withstanding extreme environments.

1. Introduction

To tackle the climate challenge and reach net zero-emission by 2050, many efforts have been made to accelerate the decarbonization of industrial processes. These energy-intensive processes are the top priority of decarbonization. Particularly, ceramic manufacturing is one of those energy-intensive processes and produces over 400 Mt CO_2 emission per year (Furszyfer Del Rio et al., 2022). The high-temperature firing process in the ceramic industry typically takes hours to days (Liu et al., 2020), and it consumes over 182 TW h (TWh) of energy per year globally, representing 75% of the ceramic manufacturing energy cost (Furszyfer Del Rio et al., 2022; Jouhara et al., 2021). Indeed, half of the United States' greenhouse gas (GHG) emissions are contributed by industrial heating (Energy.gov, 2022). Decarbonizing high-temperature processes during ceramic manufacturing is paramount to the net-zero-emission goal in 2050.

The Department of Energy (DOE) has identified three key methods to facilitate the decarbonization of industrial heat, which are particularly relevant for high-temperature processes in the ceramic industry (Energy.gov, 2022). These methods include the electrification of heat operations, the integration of low-emission heat sources, and the development and adoption of emerging low- or no-heat process technologies. Recently, electrified thermal energy sources have been used to improve the manufacturing efficiency of ceramic production. For example, ultrafast high-temperature sintering (UHS) was developed based on joule-heating, which demonstrated a high production rate and decent energy efficiency, and it is also compatible with AM processes (Wang et al., 2020). However, due to the conformal "outside-in" energy delivery mechanism, the size of the manufacturable ceramic structure by UHS is limited. As a matter of fact, the energy consumption and equipment cost would unavoidably increase with the manufacturing scale and geometry complexity of the parts because of heavy dependence on an external energy source to induce phase transformation and consolidation. While low-emission heat sources like solar heating are generally too weak for ceramic consolidation (Albrecht et al., 2016), the low- or no-heat process is promising to enable more environmentally friendly and efficient ceramic manufacturing.

Self-propagating high-temperature synthesis (SHS) is a low-heat process that utilizes the raw materials' internal chemical energy to facilitate rapid phase transition with a self-sustaining reaction wave

* Corresponding author. Department of Materials Science and Engineering, Texas A&M University, College Station, TX, 77843, USA.
E-mail address: s.wang@tamu.edu (S. Wang).

https://doi.org/10.1016/j.jclepro.2024.142122
Received 22 August 2023; Received in revised form 30 January 2024; Accepted 3 April 2024
Available online 10 April 2024

(Merzhanov, 2012). SHS was first intensively studied by A.G. Merzhanov in the 1960s (Borovinskaya et al., 2017; Merzhanov, 2012), and it has been proven to be able to fabricate most of the advanced ceramics, and industrialization has been successful in commercialized products (Borovinskaya et al., 2017; Mukasyan et al., 2019). One key feature of SHS is that once the reaction among raw materials is initiated, it propagates fast throughout the mixture, forming desired products without the need for additional energy input. This makes SHS a rapid and energy-efficient approach for ceramic manufacturing (Arlington et al., 2022). Recent efforts have focused on enhancing the SHS manufacturability of ceramic parts using binder-assisted molding followed by SHS conversion (Istomin et al., 2019a, 2019b). However, the geometric complexity was significantly limited by the molding process.

Additive manufacturing (AM) provides an effective way to manufacture complex geometry while significantly promoting material efficiency and reducing transportation through on-demand and on-site production, resulting in increasing manufacturing sustainability (Eckel et al., 2016; Gopal et al., 2023). Selective laser sintering (SLS) uses a high-power laser for selective fusion of ceramic powders. The intrinsic high melting point of ceramic powders usually leads to insufficient fusion (Lakhdar et al., 2021; Yves-Christian et al., 2010). Organic binders were commonly used to assist in the production of green parts during ceramic AM, such as binder jetting (Mariani et al., 2021) and powder-based indirect laser sintering (Shahzad et al., 2013). However, they ubiquitously require long printing time and prolonged high-temperature treatment for curing, de-binding, and sintering to produce the final ceramic parts (Du et al., 2020). Polymer-derived ceramic structures can be shaped by vat photopolymerization, where the liquid photoactive preceramic polymer is selectively cured layer by layer followed by direct pyrolyze to form ceramic structures (Eckel et al., 2016). However, energy-intensive high-temperature (>1000 °C) pyrolysis of preceramic polymers could take hours. Moreover, the photochemistry design for preceramic systems is complex, and it requires strict optical property optimization, which increases the cost and limits the selection of feedstock materials. Incorporating cheap and diverse commercially available inorganic powders is extremely challenging because the light scattering by the fillers hinders direct photopolymerization and makes this process infeasible.

Merging self-sustaining reaction and AM technology could provide sustainable and geometrically complex structure-capable solutions to ceramic manufacturing. Although the self-propagating reaction of the organic compound has been successfully integrated with freeform manufacturing technologies to create geometrically tailored polymeric (Robertson et al., 2018), metal (Liu et al., 2023) and composite structures (Zhang et al., 2021a, 2021b), little research has been focused on SHS manufacturing of geometrically tailored, spatial inorganic complex-geometry structures. Most recently, a volatile polymer/-Al/Zr/Carbon powder mixture was used as ink for direct writing of ~2 mm-height simple pattern on the substrate, followed by SHS conversion to cermets (Arlington et al., 2020, 2021). However, the fabrication of complex-geometry parts or freestanding spatial structures has not been achieved. In-situ solidification is essential to produce freestanding structures and intricate geometries, as direct writing alone lacks this capability. Using volatile polymer as an ink binder also produced significant porosity, resulting in weak mechanical strength (<13 MPa). Hence, SHS-integrated additive manufacturing of geometrically complex and mechanically robust ceramic structures remains unresolved.

To build a sustainable ceramic industry and meet the needs of future ceramic manufacturing, this work demonstrated a rapid energy-efficient AM process (REAP) of complex-geometry and freestanding ceramic structures through integration of digital model-aided layer-by-layer deposition, in-situ photothermal solidification, and subsequent self-sustaining ceramization. The REAP process features a low-carbon footprint, rapid processing, and simple implementation. Briefly, the REAP process consists of two steps, including in-situ curing-synchronized preform printing, and self-sustaining reactive ceramic conversion. Photothermal-induced in-situ solidification, a low-carbon process, is used to define the shape of the ceramic preform through curing of the pre-ceramic polymer, which instantly immobilizes and cures the extrusion deposited feedstock that consists of preceramic oligomer binder and elemental reactive powders. The crosslinked preceramic polymer not only provides a mechanically robust platform that retains the structure fidelity during the reaction but also favors the mechanical properties of the final ceramic part. After printing, the self-sustaining exothermic reaction is carried out to convert the ceramic preform (green part) to the ceramic structure. This ceramization process synchronizes the pyrolysis of preceramic polymer binders and the reactive formation of printed complex ceramic structures in a time/energy-efficient way due to the fast kinetics and highly exothermic nature of the elemental reaction. Experimental results show that such a low-heat process requires only a 10 seconds heating from a common 192W resistive heating device to initiate, and the reaction can propagate through the entire part at the speed of ~130 cm/min without the presence of additional energy input, thereby making the energy consumption of the process independent on the part geometry and size. Consequently, the ceramization reaction significantly reduced energy consumption and manufacturing time, achieving a 1000-fold decrease compared to conventional furnace sintering for a 100 cm^3 part. This reduction is anticipated to be even more substantial when manufacturing larger structures. Notably, this REAP demonstrates an exceptionally low manufacturing carbon footprint with a greenhouse gas (GHG) emission of 2.23 kg CO_2 equivalent/kg, representing 3 orders of magnitude smaller than typical binder jetting ceramic AM. Moreover, the case study also demonstrates that REAP could fabricate complex structured heat exchangers with good performance. These results demonstrated that the REAP approach shows promise for highly efficient ceramic manufacturing and could be potentially useful in advanced thermal management applications. An energy-efficient and rapid manufacturing process like this could catalyze the creation of an efficient and sustainable ceramic manufacturing industry.

2. Approach: design and implementation of REAP

A unique reactive feedstock composition was designed by combining inorganic reactive powders with pre-ceramic organic binders. Specifically, commercially available reactive elemental powders including titanium (Ti), silicon (Si) and graphite (C), and polycarbosilane-based preceramic oligomers were mixed homogeneously to produce reactive feedstock (Fig. 1a). Preceramic oligomers tuned the rheologic behavior of the feedstock for excellent printability. Moreover, upon digitally controlled extrusion, UV light-induced photothermal effect can be easily applied for in-situ curing of reactive feedstock through the thermally activated crosslinking reaction of polycarbosilane preceramic oligomers, which defined the geometry of the reactive ceramic preform (Fig. 1b). Under completion of the preform printing, the resultant green structure was converted to desired ceramic structures by the self-sustaining reaction process. With a single-point thermal trigger, exothermic reactions among the ingredients including Ti+C→TiC and 3Ti + Si+2C → Ti_3SiC_2 rapidly pyrolyzed the preceramic polymers leaving consolidated ceramic parts with desired structure (Fig. 1c). Fig. 1d and Supplementary Video 1 captured the self-sustaining ceramization of a honeycomb structure ceramic preform. Noticeably, the self-sustaining ceramization reaction proceeded from the triggering point and spread throughout the entire structure, rapidly and steadily transforming the printed preform into ceramic.

Supplementary data related to this article can be found online at https://doi.org/10.1016/j.jclepro.2024.142122

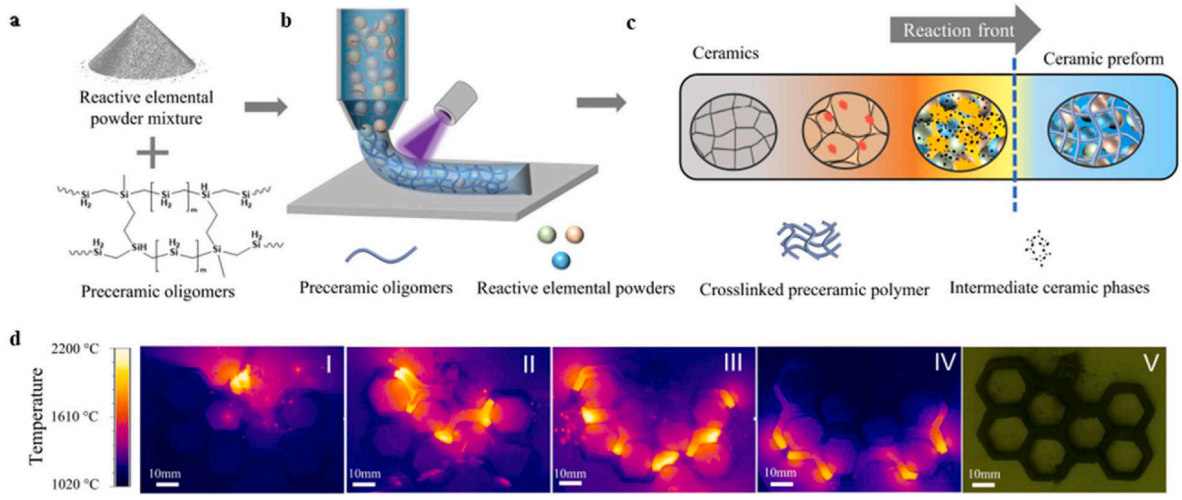

Fig. 1. Self-sustaining ceramization integrated freeform manufacturing of ceramics. a-c, Schematic illustration of the REAP process. Reactive elemental powders and preceramic oligomer mixture were directly used for the subsequent printing process. **b,** Extrusion, and in-situ photothermal solidification-based 3D printing process. **c,** Self-sustaining ceramization was triggered on the printed ceramic preform, converting the printed preform into ceramics. **d**, Thermal images of a living self-sustaining ceramization process of a honeycomb ceramic preform sample.

3. Results and discussion

3.1. Freeform fabrication of ceramic preform

The reactive feedstock was carefully designed for subsequent freeform manufacturing processes, including extrusion-based layer-by-layer deposition and in-situ photothermal solidification. SMP10, a commercially available polycarbosilane-based resin, was selected to prepare the binder for microscale powder reactants because of its good processibility and high ceramic yield after pyrolysis (Al-Ajrash et al., 2021; Wang et al., 2019). The rheological behavior of the reactive feedstock is critical for its storage and processibility. However, the as-purchased SMP10 cannot be readily used as a reactive feedstock binder due to poor rheological behavior, which can be attributed to the intrinsic low molecular weight oligomers' lack of chain configuration dynamics. To prepare the binder, SMP10 was heat treated at 155 °C for 10 min. The simple heat treatment can activate crosslinking reactions so that polymer chain entanglement and disentanglement can be induced under dynamic shearing conditions (Pratt, 2018). As a result, the micro-powder integrated preceramic polymer exhibited the desired shear thinning behavior and was ready for printing (Fig. 2a). Furthermore, in-situ photothermal curing of the as-deposited reactive feedstock

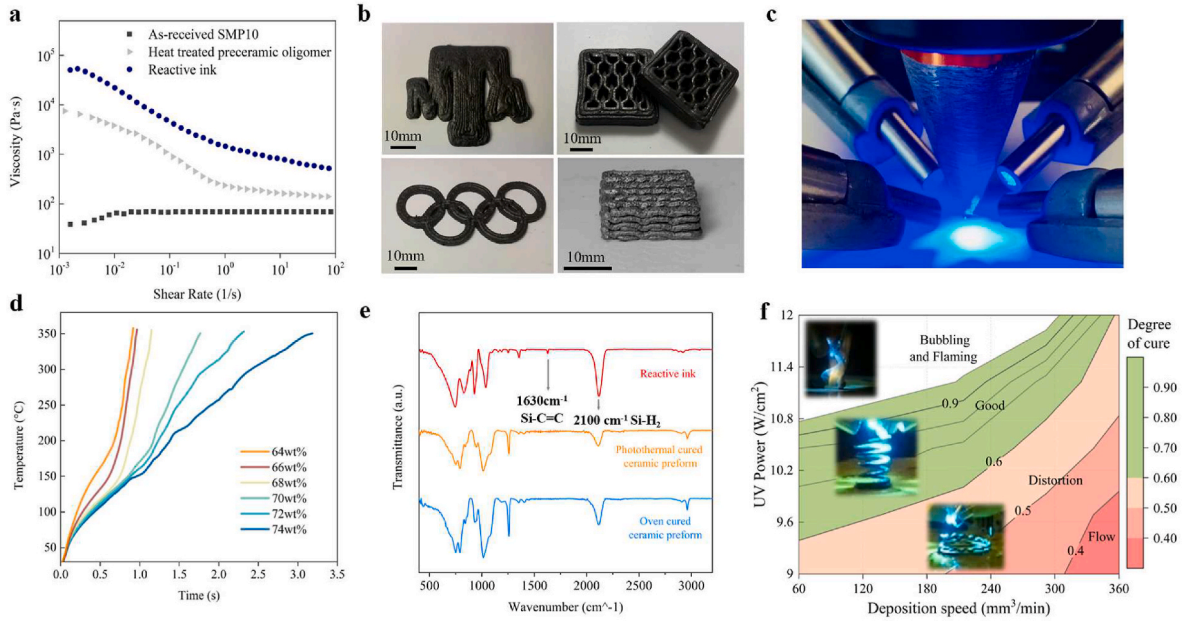

Fig. 2. Freeform fabrication of ceramic preforms through extruding and in-situ curing of reactive feedstock. a, Rheological behavior of as-received SMP10, heat-treated SMP-10, and reactive feedstock. **b,** 3D printed ceramic preforms of (I) Texas A&M University logo; (II) Honeycombs; (III) Olympics rings; and (IV) Cellular structures. **c,** UV-assisted 3D printing nozzle setup. **d,** The temperature profile of the reactive feedstock loaded with different amounts of micro-powders upon irradiation by 13W/cm^2 UV light. **e,** FTIR spectra of the reactive feedstock, photothermally cured preform, and oven-cured preform. **f,** Ceramic preforms processing map illustrating the degree of cure corresponding to printing speed and UV power condition. The green color region (degree of cure ~0.6-1) indicates good printability with a well-defined and self-stranding structure, as opposed to the printed strand being bubbling and flaming (white), distorted (light orange), and flow (dark orange). (For interpretation of the references to color in this figure legend, the reader is referred to the Web version of this article.)

enabled the REAP process to fabricate a variety of complex geometries with high fidelity (Fig. 2b). UV irradiation located near the nozzle (as shown in Fig. 2c) produced sufficient heat through photothermal effect to rapidly cure the deposited reactive feedstock without requiring the use of any photoinitiator. This photothermal curing process differs significantly from traditional direct photopolymerization, which relies on photoinitiators to generate radicals and initiate polymerization. Instead, in photothermal curing, UV-induced heat is utilized to activate preceramic crosslinking. The rate of heating was found to be dependent on the concentration of micro-powders. As shown in Fig. 2d–a series of micro-powder loading ranging from 64 wt% to 74 wt% under the 13W/cm^2 UV exposure demonstrated different photothermal heating rates ranging from 130 °C/s to 320 °C/s, which promptly raised the temperature of as-deposited layers to reach the onset temperature of binder curing (200 °C according to Supplementary Fig. 1) within 1.5 s. With increasing loading of micro-powders, the photothermal heating rate of the reactive feedstock decreases due to decreased UV absorption from preceramic polymer (Supplementary Fig. 2). The UV light absorption of reactive feedstock falls in the range of 300 nm–325 nm, and the absorption is weakened as the concentration of UV-absorbing binders decreased, which reduced the light-heat conversion efficiency (Wang, 2019). Notably, while low micro-powder loading favors a higher heating rate, which translates to a higher printing speed, the subsequent reactive ceramization process and final part performance could be undermined because insufficient reactants and excessive binders could induce excessive porosity and defects. In this case, high micro-powder loading was preferred for better ceramic performance, so specimens having 26 wt% preceramic polymer binders were selected for subsequent studies unless otherwise mentioned. To understand the UV photothermal effect-induced solidification, the reactive feedstock, photothermally cured preform, and oven-cured preform specimens were investigated by Fourier transform infrared (FTIR) spectroscopy. The peak at around 1630 cm^{-1} corresponds to the vibration of the silicon-allyl (Si–C═C) bonds, and the absorption peak of the silicon-hydrogen (Si–H) bond is located at around 2100 cm^{-1}. Fig. 2e shows the disappearance of the 1630 cm^{-1} peak and reduced intensity of peak upon UV irradiation, suggesting effective crosslinking of polymer structures through the hydrosilylation process between Si–C═C double bond and hydrogens on silicon atoms. Similar changes were also observed on the oven-cured specimen, indicating that UV-induced photothermal curing showed the same effect as conventional oven curing. To better understand the dynamics of free-form fabrication, systematic printing experiments were conducted to understand how the UV power and the printing speed affect the fabrication. A processing map of this REAP process was constructed as shown in Fig. 2f. It was found that the UV power and printing speed synergistically affect the quality of print. At high deposition speed and low UV power, the processability falls in the lower right corner regime where the feedstock tends to flow upon extrusion. The insufficient amount of photothermal heat results in a low degree of cure <0.4. The situation can be improved by increasing the UV powder or decreasing the deposition speed. This will increase the light absorption of the feedstock so that a stronger photothermal effect would induce a higher degree of cure. When the degree of cure falls between 0.4 and 0.6, the feedstock material can be solidified but with limited strength, making it difficult to print the freestanding spatial structure, which was significantly distorted. Further increase in the UV power or decrease in the deposition speed improves the fidelity where the extruded feedstock is in-situ solidified, resulting in a 'Good' region with a degree of cure greater than 0.6. However, overexposure to UV irradiation could lead to bubbling and flaming of the feedstock, which can be attributed to the overheating of flammable oligomers. Furthermore, it has been observed that increasing the cure degree of the ceramic preform results in reduced porosity (Supplementary Table 1). Printing at a speed of 80~120 mm^3/min and UV power 10.8 of results in a degree of cure greater than 90% and a final porosity of ~26%. This configuration, which yields the lowest porosity, is adopted for subsequent studies and structure fabrication unless specified otherwise. Therefore, careful calibration of the UV power and deposition speed is necessary to achieve optimal fidelity and mechanical performance of the ceramic preform and final ceramic structure. With precise control of deposition rate and UV irradiation power, the synchronization of deposition process and curing rate allows REAP to fabricate high-fidelity complex shapes, including freestanding overhanging structures (Supplementary Video 2).

Supplementary data related to this article can be found online at https://doi.org/10.1016/j.jclepro.2024.142122

3.2. Self-sustaining ceramization characteristics

REAP is unique in its ability to manufacture ceramics rapidly and energy-efficiently with a self-sustaining ceramization reaction. The whole ceramization process requires negligible energy because transient thermal energy was supplied by a tungsten heater (192 W) for less than 10 s, and the rest of the reaction does not need additional external energy input. Therefore, the ceramization reaction only requires less than 2000 J energy input to complete. Fig. 3a shows the time-resolved thermal images of the propagation of a typical self-sustaining ceramization reaction that transforms the preform into ceramics. The reaction was marked by a fast and steadily propagating front with a high front temperature. Thermochemical simulation of the self-sustaining ceramization reaction using the finite element method provided useful insight into the process. The simulated reaction results are shown in Fig. 3b, which were consistent with the experimental observations. The temperature profiles of the experimental and simulated self-sustaining reaction are compared in Fig. 3c. The mean absolute percentage error (MAPE) was calculated to be 2.6%, indicating good agreement between the two curves. The unique self-sustaining reaction feature could be attributed to the delicate balance among the fast exothermic reactions of elemental powders, pyrolysis of preceramic polymers by transient high reaction enthalpy, and dynamic heat transfer within the system as shown in Supplementary Fig. 3. As a result, the reaction front temperature, ranging from 1979 °C to 2400 °C, was strongly dependent on the content of preceramic polymer binder (Fig. 3d). As the binder concentration increased, the higher amount of binders required more heat for pyrolysis, resulting in a reduction in the reaction front temperature. The pyrolysis of organic binder would unavoidably leave pores within the structure and thus could compromise the mechanical properties of the part. On the other hand, the reaction propagation velocity was less influenced by the preceramic polymer fraction. The results indicate that less preceramic polymer binder might be desirable for high part quality. The final ceramic structure demonstrated excellent fidelity with the printed preforms after the self-sustaining ceramization (Supplementary Fig. 4).

3.3. Self-sustaining ceramization mechanism

To elucidate the mechanism of the rapid phase transformation of the ceramization process, the phase evolution during the reaction was characterized by X-ray Diffraction (XRD), and the results of the specimens at different stages of the reaction are shown in Fig. 4a. A schematic illustration of the 4 reaction stages is shown in Supplementary Fig. 5. XRD spectra were analyzed using Rietveld refinement for phase identification. Supplementary Fig. 6 shows the detailed results with reference to the JCPDS database. Specifically, before the reaction was initiated, the XRD spectrum at t_1 shows that the ceramic preform only contains phases that correspond to the elemental powder Ti, Si, and graphite, which suggests that the preform printing process did not introduce detectable reactions among elemental particles. As the reaction front approaches the spot (at t_2), unreacted feedstock was first heated by the propagating high temperature front. The formation of the TiC phase was first observed by the pre-heating at t_2. After the reaction front crossed the spot, it automatically propagated until cooling down. During the

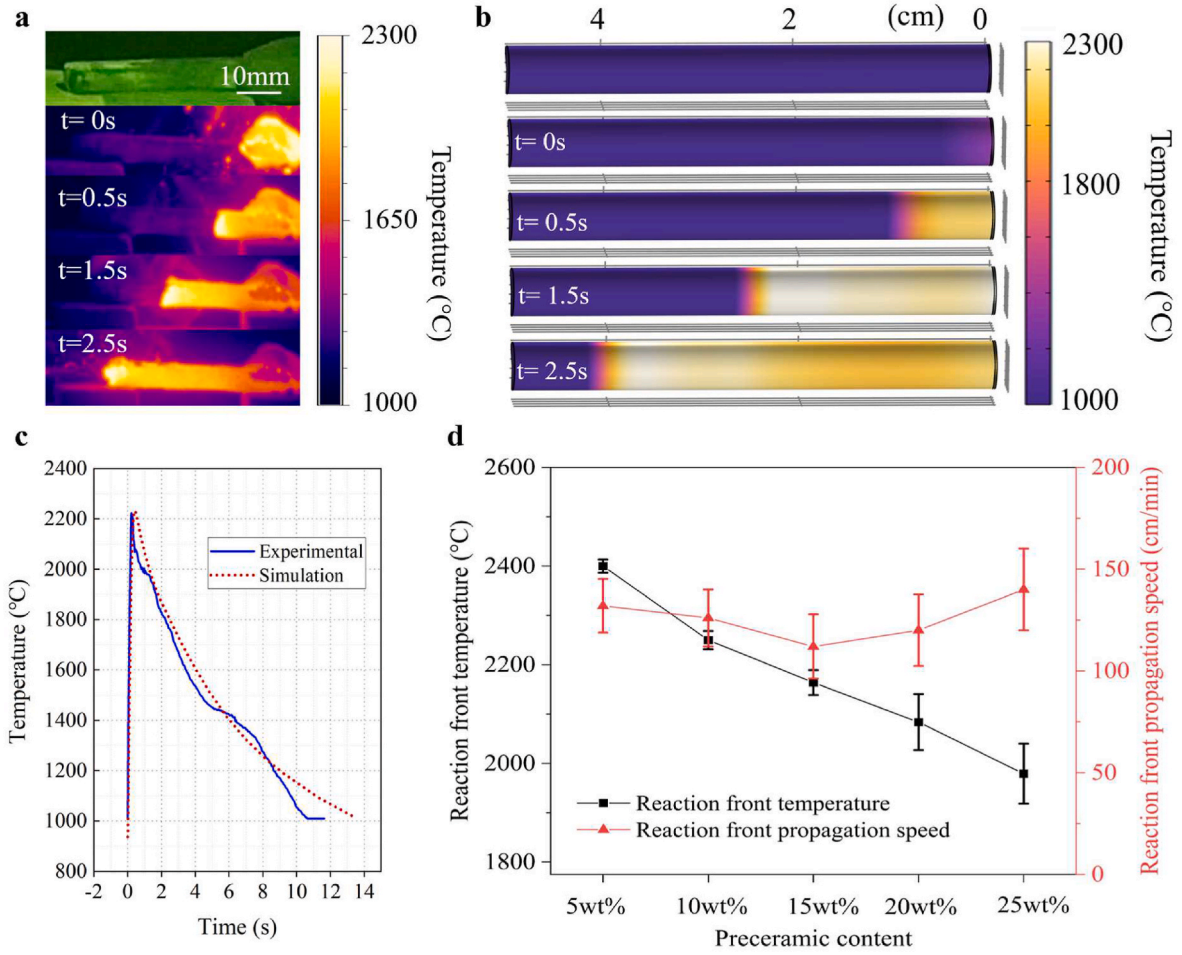

Fig. 3. Self-sustaining ceramization characteristics. a, experiment, and **b,** simulation. **c,** Comparison of experimental measured and modeled self-sustaining ceramization temperature profile. **d,** Self-sustaining ceramization characteristics of the ceramic preform with different preceramic polymer content.

post-front reaction stage at t_3, the elemental phases were essentially consumed, and the TiC phase remained along with other intermediate phases. At t_4, the specimen cooled down to room temperature naturally. The Ti_3SiC_2 phase can be identified by both XRD and TEM analysis (Supplementary Fig. 7), indicating the majority of the Ti_3SiC_2 phase formed during the cooling stage. The results are consistent with the previous studies (Gauthier et al., 2006; Meng et al., 2013) indicating that Ti_3SiC_2-based ceramic composite structure was rapidly produced during self-sustaining ceramization. To help better understand the different-stage phase evolution, the temperature profile was characterized, as shown in Fig. 4b. In the temperature profile, each stage corresponding to XRD analysis was marked as t_1, t_2, t_3, and t_4. SEM images of the ceramic preform before and after self-sustaining ceramization are shown in Fig. 4c and d, respectively.

It was also noticed that the preceramic polymer integrated REAP approach could produce parts with a low porosity of 25.6%, marking a 60% reduction in porosity compared to its reactively fabricated inorganic counterpart (Arlington et al., 2021). The preceramic polymer is crucial in obtaining the low porosity ceramic structure, contrasting with the outcomes observed in previous studies where volatile polymers such as cellulose acetate (Arlington et al., 2021) and polyvinyl alcohol (Istomin et al., 2019a) are utilized as binders in the reactive synthesis of inorganic materials. In those cases, maintaining geometric accuracy often requires external pressure or molds, and the structure can still be distorted during self-sustaining reactions (Istomin et al., 2019b). Additionally, a high porosity of up to 66.4 % is typically observed due to the complete decomposition of these volatile polymers during the conversion process at high temperatures (Arlington et al., 2021). In contrast, the polycarbosilane polymer in our formulation first undergoes a curing process to form a cross-linked skeleton, effectively binding the reactive powder. This skeleton provides structural integrity during the subsequent pyrolysis stage, where it is converted into stable SiC ceramic structures. This chemical process is illustrated in Supplementary Fig. 8. The formation of silicon carbide (SiC) from polycarbosilane is indicated in the X-ray diffraction (XRD) results shown in Fig. 4a. Here, SiC appears at time point t_2, which is an early stage of a self-sustaining reaction. This formation of SiC at such an early stage is not observed in systems that do not contain a polycarbosilane binder (Riley et al., 2008). However, pores and small holes are also observable in the SEM image (Supplementary Fig. 9), this can be mainly attributed to the escaping of volatile substances during quick pyrolysis.

3.4. *Manufacturing efficiency*

REAP could transform the ceramic manufacturing industry with an energy-efficient and high-rate fabrication route. The energy consumption and consolidation time of the self-sustaining ceramization approach were compared to both conventional and state-of-the-art methods, and the results are shown in Fig. 5a. Compared to the conventional furnace-based firing processes, the energy consumption of the self-sustaining ceramization for unit volume of ceramic consolidation decreased by 1000 times. In our case, admittedly, the embodied energy in the reactive elemental powders is nontrivial. For example, embodied energy for pure titanium production through atomization is 31.7 MJ/kg (Lyons et al.,

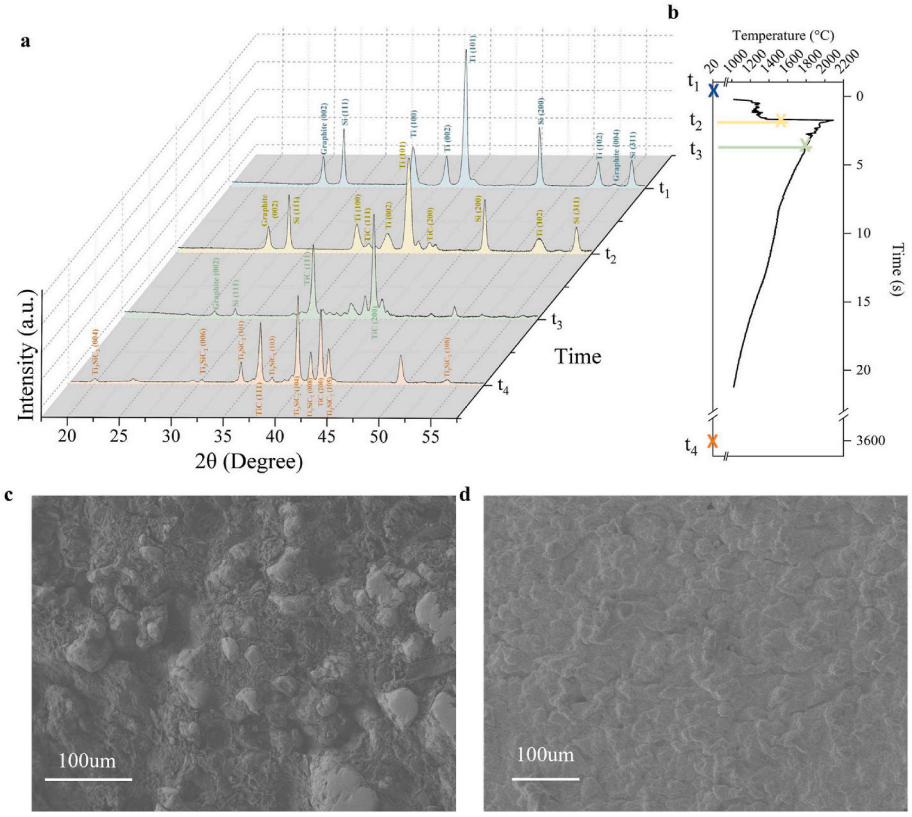

Fig. 4. Self-sustaining ceramization mechanism. a, XRD spectra of specimens at different stages of ceramization reaction, at t_1, the reaction is not initiated, and the specimen is at room temperature; preheating stage t_2 is immediately ahead of the reaction front; reacting stage t_3 is ~2 s after reaction front; and at t_4, the specimen is naturally cooled after reaction complete. **b,** the temperature profile of self-sustaining ceramization where t_2 and t_3 correspond to preheating stage and reacting stage, respectively. **c,** SEM image of the ceramic preform at t_1 **d**, SEM image of ceramic structure at t_4.

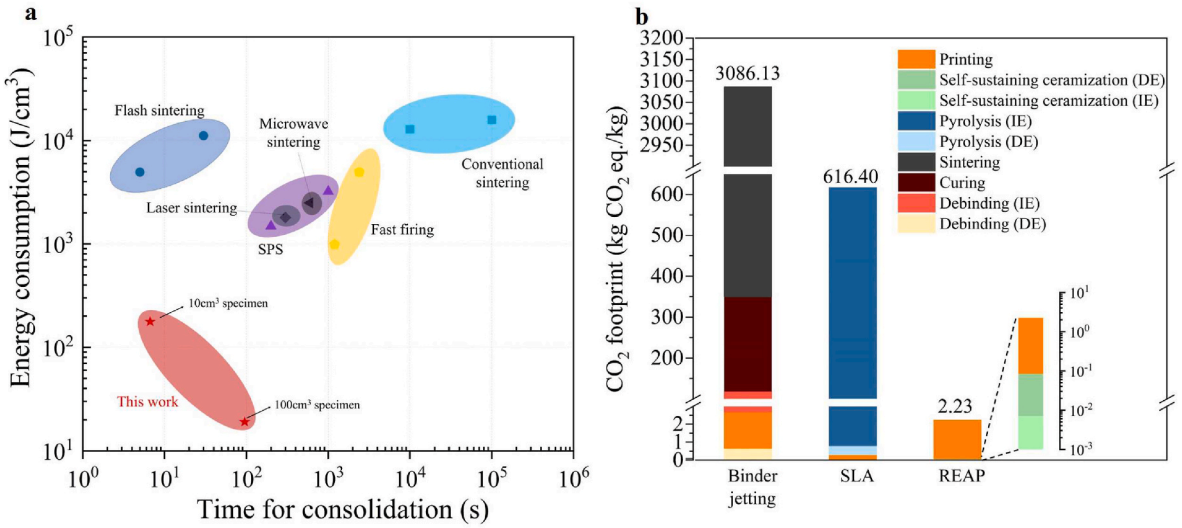

Fig. 5. Manufacturing efficiency. a, Manufacturing efficiency of the self-sustaining ceramization method compared to other ceramic consolidation methods in terms of specific energy consumption and duration of consolidation [38]. **b,** CO_2 emission footprint of REAP compared to representative ceramic additive manufacturing technologies (Krüger, 2020; Mariani et al., 2021; Meteyer et al., 2014; Xu et al., 2015; Yves-Christian et al., 2010). DE and ID represent direct emission and indirect emission, respectively.

2021). On the other hand, however, fabrication of the raw materials for alternative traditional pressureless sintering could also be energy intensive. For example, the embodied energy for TiC is considered to be significant due to the utilization of energy-costly magnesium (Mhadhbi and Driss, 2021). Nonetheless, the focus of our study is on the energy efficiency of the manufacturing processes, including forming and consolidation. Therefore, embodied energy analysis is beyond the scope of this paper.

Interestingly, the normalized energy consumption of REAP was 192 J/cm^3 in manufacturing a 10 cm^3 part, while it was almost 10-fold less in

manufacturing a 10-fold larger part (100 cm^3), as low as 19.2 J/cm^3. Since the initiation (192 W thermal heating for 10 s) is the only energy input for ceramization, the energy efficiency advantage scales with the size of the part. Due to the fast kinetics of the self-sustaining ceramization reaction, the consolidation of a 10 cm^3 sample only took 5 seconds, 1000 times faster than conventional sintering. Moreover, the environmental impact of REAP was analyzed in comparison with a typical vat photopolymerization process, stereolithography (SLA), and binder jetting ceramic AM technologies in terms of equivalent CO_2 emission. The results are shown in Fig. 5b. Detailed description of the calculation was provided in Supplementary Note 1. The calculation indicated that the SLA showed 616.40 kg equivalent CO_2 emission in producing one kg ceramic and the binder jetting process emitted equivalent 3086.13 CO_2/kg. In contrast, REAP exhibited an exceptionally low carbon footprint of only 2.23 kg CO_2 equivalent/kg since it does not involve carbon-intensive pyrolysis or sintering steps. These findings suggest that REAP demonstrated in this work could be disruptive in shaping the efficiency and sustainability of ceramic manufacturing.

3.5. Case study: REAP manufacturing of heat exchanger for waste heat recovery

In this section, we fabricate and evaluate a geometrically tailored ceramic heat exchanger (HX) to demonstrate the remarkable application-oriented manufacturing capabilities of REAP for complex-geometry ceramic structures. A heat exchanger (HX) is an economical and efficient device for harvesting thermal energy from waste heat. It enables industries to recover and reuse wasted thermal energy, thereby increasing thermal energy efficiency. Ceramic HXs are promising in extreme environmental applications due to their high-temperature resistance and corrosion resistance(Kaur and Singh, 2021). However, the efficient manufacturing of geometrically optimized ceramic HXs remains a challenge. For instance, gyroid geometry, a complex three-dimensional structure that divides space into two interconnected regions, is well-known for its high efficiency in heat transfer, but it is impossible to fabricate such structure by conventional molding. Although the binder jetting AM process was employed to fabricate ceramic gyroid HX, solely the sintering process could take 4 days at an extremely high temperature of 1900 °C, and the heat exchange performance is still unknown (Kelly et al., 2022). Here, a proof-of-concept gyroid structured ceramic HX, with 1.5 unit cells was fabricated by REAP (Fig. 6a). The microscopic images shown in Fig. 6b reveal a seamless joining between layers, even at a tortuous topology, and no catastrophic cracks were observed. This characteristic is critical for leak-free fluid-based heat exchange (HX) operation. In addition, the porosity level influences the heat transfer efficiency, thermal conductivity, and mechanical strength of the heat exchanger, as well as the manufacturing cost. Typically, porosity levels in ceramics used in heat exchangers range from low (<5%) (Sommers et al., 2010) to moderate (22%–25%) (Velasco Gómez et al., 2005) to balance these factors effectively. Here, our objective is to demonstrate the manufacturing capabilities of the REAP process. We've achieved a porosity level of 25.6%, which could be used in heat exchangers utilized applications. The liquid-to-liquid heat exchange performance of the ceramic gyroid HX was numerically and experimentally studied for the first time. Testing setup and detailed procedures and calculations are described in Supplementary Note 2 and Supplementary Fig. 10. Experimental results in Fig. 6c show the equilibrium temperatures at each media port for the ceramic gyroid HX unit, while Fig. 6d shows the HX hardware during performance testing. The hot fluid experiences a temperature drop of 6.5 °C from its inlet for single-unit HX. Meanwhile, the cold fluid undergoes a temperature gain of 4.6 °C from its inlet. Further, the finite element model and the simulated temperature distribution in a gyroid unit cell (Supplementary Fig. 11) provide insights into the thermal dynamics within the REAP-fabricated structure, which visualize the REAP technique's capability to manufacture complex geometrical designs that facilitate such thermal dynamics. The performance of the REAP manufactured heat exchanger was also evaluated and the results are shown in Supplementary Fig. 12. Additionally, the mechanical properties of the REAP fabricated structure confirm that the REAP approach is promising for load-bearing applications like HXs. The fracture toughness and yield strength of the REAP manufactured part could reach 1.7 MPa $m^{1/2}$ and 1.8 × 10^2 MP, respectively. They are comparable to those of technical ceramic materials manufactured by other processes (Supplementary

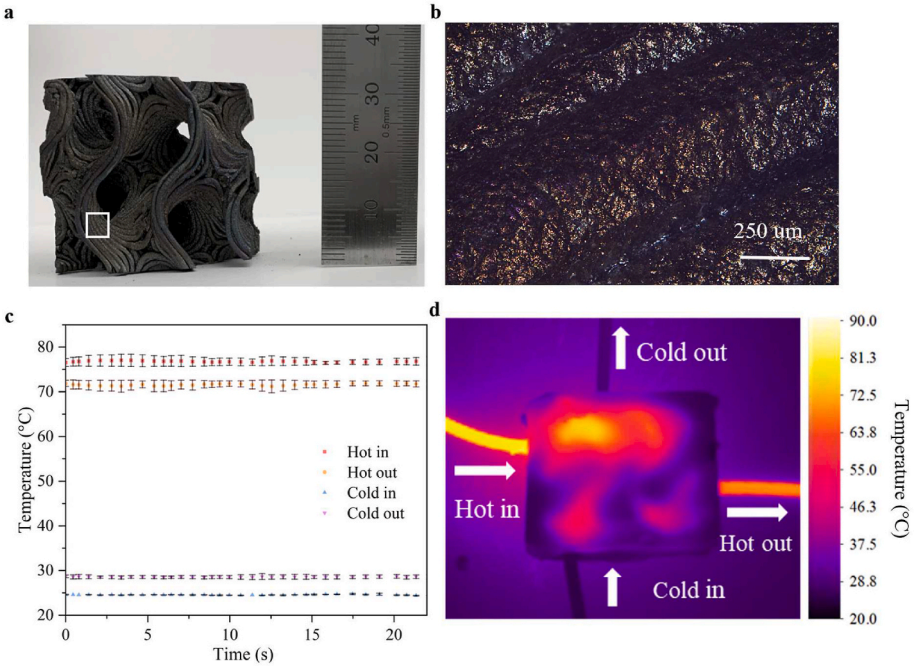

Fig. 6. REAP manufactured structures for heat exchange applications. a, Optical image of the REAP fabricated gyroid structure with a selected area of interest (within a white rectangle) magnified in **b**, optical microscope image. **c,** Experimentally measured inlet and outlet temperatures of hot and cold fluid in the gyroid heat exchanger. **d,** thermal image captured during heat exchange performance testing.

Fig. 13). The REAP approach, therefore, holds promise for a wide range of applications for manufacturing complex ceramic structures, extending its utility beyond traditional applications.

4. Materials and methods

4.1. Materials

Commercial micro-powders of silicon (Si, 325 mesh), and graphite (C, <20um) were purchased from Sigma Aldrich. Titanium powders (Ti, <20um) were purchased from Atlantic Equipment Engineers. Polycarbosilane-based preceramic oligomers (SMP10) were purchased from Starfire® Systems, Inc. A 192W Tungsten basket (EVB133030W, Kurt J. Lesker Company) was used to initiate the self-sustaining ceramization.

4.2. Preparation of reactive feedstock

The micro-powder reactants were prepared by mixing powders of Ti, Si, and graphite in a molar ratio of 3:1:2. Specifically, the mixing of powders was performed in ethanol suspension in an ultrasonication bath for 1 h followed by mechanically stirring for 1 h. To remove the ethanol, the suspension was then dried at 85 °C under mild mechanical stirring overnight until ethanol content was not detectable with differential scanning calorimetry. Before preparing the reactive feedstock, polycarbosilane-based preceramic oligomers (SMP10) were heat treated at 155 °C under vigorous stirring for 10 min to obtain the preceramic oligomer binder. A series of reactive feedstocks with different concentrations of micro-powder reactants were prepared by mixing the preceramic oligomer binder and the micro-powder reactants. For the following reactive feedstock composition-related studies, the parameters of the reactive feedstock specimen are detailed in Supplementary Table 2. Otherwise, the reactive feedstock specimen used in the tests contains 26 wt% preceramic polymers.

4.3. Rheological characterization

The rheological behavior of preceramic oligomers was characterized by Anton Paar Physica MCR-301 rheometer under the cone-and-plate mode, while the reactive feedstocks were investigated with parallel-plate mode. For reactive feedstock investigation, both top and bottom plates are covered by sandpaper to prevent wall slip.

4.4. Photothermal in-situ curing

The photothermal effect was characterized by the temperature profile of the illuminated sample using a FLIR A325sc IR thermal camera. The calibration followed our previous report steps(*Zhang* et al., *2021a*). The recorded thermograph was used for further photothermal effect analysis. Photothermal in-situ curing was carried out by Omnicure S2000, Excelitas technologies with a standard filter. The various powers, ranging from 4.5W/cm^2 to 13W/cm^2, delivered to the sample were first recorded by the radiometer and then calibrated considering the distance between the output portal and the target.

4.5. Freeform manufacturing of ceramic preform

Digitally controlled extrusion of reactive feedstock was performed on a 3D Potter model Micro 10 with a 1 mm nozzle. A four-way light guide was fixed on the nozzle area with a self-made mount for in-situ curing. The sample used for the test contains 26 wt% preceramic polymers. The degree of cure (α) for the fabricated preform was quantitatively characterized through Differential Scanning Calorimetry (DSC) tests (TA instruments Q20). Firstly, a reference feedstock was prepared and then tested by DSC from room temperature to 350 °C at a heating rate of 5 °C/min, and the heat of full reaction ΔH_{full} was obtained. Samples were obtained from different printed pieces at different locations along the direction of light illumination to characterize the degree of cure. Also, a small piece of samples from printed preforms under different printing speeds and irradiation powers were cut out and used for the DSC test. The residual heat of the reactions ($\Delta H_{residue}$) was obtained from DSC results. Then the degree of cure values for photothermal in-situ curing was calculated by the equation:

$$\alpha = 1 - \left(\frac{\Delta H_{residue}}{\Delta H_{full}}\right) \times 100\% \quad (1)$$

4.6. Self-sustaining ceramization implementation

After ceramic preforms were fabricated, they were transported to an Argon gas-filled glove box. A tungsten basket (Kurt J. Lesker Company, EVB133030W) heated by a DC power supply was used to initiate the self-sustaining reaction. The reaction temperature evolution is recorded on an Optris PI 05M infrared thermal camera. After heating the ceramic preforms for ~10 seconds, the initiation of the self-sustaining reaction can be noticed by a bright glowing of the preform after which the tungsten heater was turned off immediately. A digital camera (DJI Osmo Action with a light filter) was also installed to record the reaction. Specimens with dimensions 50mm × 5mm × 5 mm were used for reaction characteristic studies. Characteristics of the self-sustaining reaction, including reaction front temperature and reaction propagating speed, were calculated from infrared recordings that are composed of a time-resolved thermal map at a frame rate of 27Hz. The average reaction characteristic value was determined from 5 samples, and the standard deviation was represented as the error bar in the graph.

4.7. Material characterization

Scanning electron microscopy (JEOL JSM-7500F) equipped with energy-dispersive spectroscopy (EDS) at 20 kV accelerating voltage was used to perform microstructure and elemental analysis. The test of relative bulk density followed the international standard ISO 18754 (Standard ISO18754, 2013). X-ray diffraction (XRD) spectra of the ceramic part (produced from fully cured ceramic preform containing 26 wt% preceramic polymers.) were recorded on a Bruker D8 Discover diffractometer at a voltage of 40 kV and current of 40 mA with CuKα (λ: 1.5418 Å) radiation. Phase evolution of the self-sustaining ceramization study was carried out by the reaction front quenching method (Pacheco, 2007). Specifically, a copper block was placed in contact with a cuboid specimen (50mm × 5mm × 5 mm) after the reaction was initiated. The copper block quickly removed the heat away from the reacting specimen resulting in the quenching of the reaction. The quenched reaction front was identified as the location having the highest temperature. The unreacted zone located immediately after the reaction front was analyzed as the preheating zone. The identified reacting zone had been reacted for ~2 s. The specimens were analyzed by XRD and further analyzed by the Rietveld refinement method on TOPAS software to determine the phase composition.

4.8. Mechanical properties and porosity testing

Flexural strength was tested following the ASTM C1161 − 18 (ASTM International, 2023). The specimen was tested by an MTS test machine with 5 kN load cells, and the displacement of load cells was set to 0.5 mm/min. The standard cylindrical sample was mounted with 3M VHB tape to prevent horizontal movement and mitigate uneven sample surface. Fracture toughness was tested and calculated following the pre-cracked beam method from ASTM C1421 – 10 (Ceramics, 2010).

The porosity was tested in accordance with the international standard ISO 18754. The method of test followed Archimedes' principle, and the relative bulk density π_b was first calculated as, $\pi_b = (m_1 - m_2)/(m_3 - m_2) \times \rho_1$, where m_1 is the mass of the dry sample, m_2 is the apparent

mass of the immersed sample, m_3 is the mass of the soaked sample, ρ_1 is the density of the immersed liquid (Standard ISO18754, 2013). Then the porosity was obtained by $1 - \pi_b$.

4.9. Finite element simulation

The numeric modeling was carried out on COMSOL Multiphysics 6.0, a finite element analysis platform, to simulate the self-sustaining consolidation and pyrolysis process. The following equations were used to define the heat transportation and reaction kinetics of the self-sustaining ceramization process (Borovinskaya et al., 2017).

$$\rho C_p \frac{\partial T}{\partial t} = \rho H_r \frac{\partial \eta}{\partial t} + \lambda \left[\frac{\partial^2 T}{\partial r^2} + \frac{1}{r}\frac{\partial T}{\partial r} + \frac{\partial^2 T}{\partial z^2} \right] \quad (2)$$

$$\frac{\partial \eta}{\partial t} = A_0 (1-\eta) exp\left(-\frac{E_a}{RT}\right) \quad (3)$$

$$\frac{\partial \eta_d}{\partial t} = A_0 (1-\eta_d)^n \, exp\left(-\frac{E_a\_SMP}{RT}\right) \quad (4)$$

Where T is the temperature in Kelvin (K); η represents the degree of conversion of reactant powders and is dimensionless; ρ, *and* C_p denotes density and heat capacity of the powder reactants, respectively; H_r is the enthalpy of reaction for Ti–Si–C system. In equation (3), the conversion rate $\frac{\partial \eta}{\partial t}$ for the Ti–Si–C system is described. A_0 is the reaction rate constant, (1- η) is used here as the conversion function; E_a *and* R respectively are the activation energy and universal gas constant. In equation (4), the rate of decomposition for preceramic polymers $\frac{\partial \eta_d}{\partial t}$ is described. The value and source of constants in the equation used in COMSOL software are listed in Supplementary Table 3. The convective and surface-to-ambient radiation boundary conditions are applied to all surfaces while the main body of the model is treated as a heat source that releases heat according to equations (3) and (4). A default relative tolerance of 0.01 is applied. The thermal conductivity of the ceramic preform was measured by Hot Disc thermal conductivity analysis. The heat capacity was obtained from DSC (TA instruments Q20). The density of the ceramic preform was measured from a standard sample by taking the mass divided by the volume of the sample. The yield of Ti_3SiC_2 (36%) was considered based on XRD results.

4.10. Manufacturing efficiency calculation

Calculation of the energy consumption of different consolidation techniques was performed by normalizing data from previous studies (Sohrabi Baba Heidary et al., 2018) by the dimensions of the specimen (Stawarczyk et al., 2013). The detailed calculation of GHG emission of different ceramic AM technology can be referred to Supplementary Note 1 and Supplementary Table 5. 0.000120 $kgCO_2$-eq/kJ was used as the GHG emissions factor to convert energy consumption into carbon dioxide equivalent (Ibn-Mohammed et al., 2019).

4.11. Heat exchanger characterization

Detailed heat exchanger performance tests, related calculations, and implementation of numerical simulation can be found in Supplementary Note 2.

5. Conclusion and future works

In this work, we report a rapid and energy-efficient approach for freeform manufacturing of ceramic structures through creatively integrating in-situ photothermal curing and ex-situ self-sustaining ceramization. Photothermal in-situ solidification was synchronized with the extrusion-based printing of micro-powders-filled preceramic oligomer feedstock to ensure high fidelity with the computer model. After printing, self-sustaining ceramization, a low-heat reaction process, was initiated to convert the ceramic preform to the ceramic structure without needing external energy except for the initiation. The ceramization synchronizes the pyrolysis of preceramic polymer and reactive formation of desired ceramic structure in a time and energy-efficient fashion. REAP demonstrates a 192 J/cm^3 energy consumption and 10-s consolidation time, both 100-fold more efficient than conventional processes. The rapid and low carbon footprint nature of REAP is built on the efficient utilization of feedstock materials' internal chemical energy, which facilitates a quick reaction to produce desired ceramic products and simultaneously pyrolyze preceramic binders. Particularly, the carbon footprint of REAP was calculated to be 1000-fold less than binder jetting ceramic printing. The REAP was also demonstrated in manufacturing geometrically tailored ceramic composite heat exchangers.

Future research will prioritize several key areas to advance REAP technology. Firstly, cost-effective and environmentally friendly binders will be explored to enhance sustainability and accessibility. Secondly, efforts will be made to expand the variety of ceramic materials compatible with the REAP process, broadening its application scope. Lastly, studies on the unknown properties of materials produced through REAP, such as thermal and electrical characteristics, will be conducted. These steps are essential for addressing current limitations and fully leveraging the potential of REAP in additive manufacturing.

Overall, this new approach has the potential to revolutionize the manufacturing process of complex-geometry ceramic composite structures, offering rapid production and energy efficiency.

CRediT authorship contribution statement

Ruochen Liu: Conceptualization, Data curation, Formal analysis, Investigation, Methodology, Writing – original draft, Writing – review & editing. **Aolin Hou:** Investigation. **Prashant Dhakal:** Investigation. **Chongjie Gao:** Investigation. **Jingjing Qiu:** Project administration, Writing – review & editing. **Shiren Wang:** Conceptualization, Funding acquisition, Methodology, Project administration, Resources, Supervision, Writing – review & editing.

Declaration of Competing Interest

The authors have filed a patent application.

Data availability

Data will be made available on request.

Appendix A. Supplementary data

Supplementary data to this article can be found online at https://doi.org/10.1016/j.jclepro.2024.142122.

References

ASTM International, 2023. C1161-18: Standard Test Method for Flexural Strength of Advanced Ceramics at Ambient Temperature. ASTM International, West Conshohocken, PA, USA.
Al-Ajrash, S.M.N., Browning, C., Eckerle, R., Cao, L., 2021. Initial development of preceramic polymer formulations for additive manufacturing. Materials Advances 2 (3), 1083–1089.
Albrecht, A., Rivadeneyra, A., Abdellah, A., Lugli, P., Salmerón, J.F., 2016. Inkjet printing and photonic sintering of silver and copper oxide nanoparticles for ultra-low-cost conductive patterns. J. Mater. Chem. C 4 (16), 3546–3554.
Arlington, S.Q., Barron, S.C., DeLisio, J.B., Rodriguez, J.C., Vummidi Lakshman, S., Weihs, T.P., Fritz, G.M., 2021. Multifunctional reactive nanocomposites via direct ink writing. Advanced Materials Technologies 6 (5), 2001115.
Arlington, S.Q., Fritz, G.M., Weihs, T.P., 2022. Exothermic Formation reactions as local heat sources. Annu. Rev. Mater. Res. 52, 219–248.
Arlington, S.Q., Lakshman, S.V., Barron, S.C., DeLisio, J.B., Rodriguez, J.C., Narayanan, S., Fritz, G.M., Weihs, T.P., 2020. Exploring material chemistry for direct ink writing of reactively formed conductors. Materials Advances 1 (5), 1151–1160.

Borovinskaya, I.P., Gromov, A.A., Levashov, E.A., Maksimov, Y.M., Mukasyan, A.S., Rogachev, A.S., 2017. Concise Encyclopedia of Self-Propagating High-Temperature Synthesis: History, Theory, Technology, and Products. Elsevier.
Ceramics, A.C.o.C.o.A, 2010. Standard Test Methods for Determination of Fracture Toughness of Advanced Ceramics at Ambient Temperature. ASTM International.
Du, W., Ren, X., Pei, Z., Ma, C., 2020. Ceramic binder jetting additive manufacturing: a literature review on density. J. Manuf. Sci. Eng. 142 (4), 040801.
Eckel, Z.C., Zhou, C., Martin, J.H., Jacobsen, A.J., Carter, W.B., Schaedler, T.A., 2016. Additive manufacturing of polymer-derived ceramics. Science 351 (6268), 58.
Energy.gov, 2022. Energy earthshots – U.S. Department of energy industrial heat Shot™. https://www.energy.gov/sites/default/files/2022-09/earth-shot-industrial-heat-fact-sheet.pdf.
Furszyfer Del Rio, D.D., Sovacool, B.K., Foley, A.M., Griffiths, S., Bazilian, M., Kim, J., Rooney, D., 2022. Decarbonizing the ceramics industry: a systematic and critical review of policy options, developments and sociotechnical systems. Renew. Sustain. Energy Rev. 157, 112081.
Gauthier, V., Cochepin, B., Dubois, S., Vrel, D., 2006. Self-propagating high-temperature synthesis of Ti3SiC2: study of the reaction mechanisms by time-resolved X-ray diffraction and infrared thermography. J. Am. Ceram. Soc. 89 (9), 2899–2907.
Gopal, M., Lemu, H.G., Gutema, E.M., 2023. Sustainable additive manufacturing and environmental implications: literature review. Sustainability 15 (1), 504.
Ibn-Mohammed, T., Randall, C., Mustapha, K., Guo, J., Walker, J., Berbano, S., Koh, S., Wang, D., Sinclair, D., Reaney, I., 2019. Decarbonising ceramic manufacturing: a techno-economic analysis of energy efficient sintering technologies in the functional materials sector. J. Eur. Ceram. Soc. 39 (16), 5213–5235.
Istomin, P., Istomina, E., Nadutkin, A., Grass, V.J.R., Ceramics, I., 2019a. Production of Multichannel Ceramics Based on Ti 3 SiC 2, 60, pp. 264–267, 3.
Istomin, P., Nadutkin, A., Istomina, E., Grass, V., 2019b. Synthesis of Ti3SiC2 MAX phase ceramic materials using macrosized non-powder forms of titanium metal. In: IOP Conference Series: Materials Science and Engineering. IOP Publishing, 012015.
Jouhara, H., Bertrand, D., Axcell, B., Montorsi, L., Venturelli, M., Almahmoud, S., Milani, M., Ahmad, L., Chauhan, A., 2021. Investigation on a full-scale heat pipe heat exchanger in the ceramics industry for waste heat recovery. Energy 223, 120037.
Kaur, I., Singh, P., 2021. State-of-the-art in heat exchanger additive manufacturing. Int. J. Heat Mass Tran. 178, 121600.
Kelly, J.P., Finkenauer, L.R., Roy, P., Stolaroff, J.K., Nguyen, D.T., Ross, M.S., Hoff, A.T., Haslam, J.J., 2022. Binder jet additive manufacturing of ceramic heat exchangers for concentrating solar power applications with thermal energy storage in molten chlorides. Addit. Manuf. 56, 102937.
Krüger, C., 2020. CO2 Emissions of Pyrolyzed Mixed Plastic Waste and the Mass Balance Approach. BASF.
Lakhdar, Y., Tuck, C., Binner, J., Terry, A., Goodridge, R., 2021. Additive manufacturing of advanced ceramic materials. Prog. Mater. Sci. 116, 100736.
Liu, R., Gao, C., Hou, A., Wang, S., 2023. Ni/Al foil-based reactive additive manufacturing with fast rate and high energy-efficiency. J. Mater. Process. Technol. 321, 118167.
Liu, Y., Sun, B., Shu, Y., Zeng, X., Zhu, J., Yi, J., He, J., 2020. Preparation of superior IGZO ceramics by two-step sintering for application in IGZO thin film fabrication. J. Mater. Res. Technol. 9 (3), 5331–5342.
Lyons, R., Newell, A., Ghadimi, P., Papakostas, N., 2021. Environmental impacts of conventional and additive manufacturing for the production of Ti-6Al-4V knee implant: a life cycle approach. Int. J. Adv. Des. Manuf. Technol. 112, 787–801.
Mariani, M., Beltrami, R., Brusa, P., Galassi, C., Ardito, R., Lecis, N., 2021. 3D printing of fine alumina powders by binder jetting. J. Eur. Ceram. Soc. 41 (10), 5307–5315.
Meng, F., Liang, B., Wang, M., 2013. Investigation of formation mechanism of Ti3SiC2 by self-propagating high-temperature synthesis. Int. J. Refract. Metals Hard Mater. 41, 152–161.
Merzhanov, A.G.e., 2012. 40 YEARS of SHS: A LUCKY STAR of A SCIENTIFIC DISCOVERY A Presentation with Elements of a Scientific Lecture. Bentham Science Publishers.
Meteyer, S., Xu, X., Perry, N., Zhao, Y.F., 2014. Energy and material flow analysis of binder-jetting additive manufacturing processes. Procedia Cirp 15, 19–25.
Mhadhbi, M., Driss, M., 2021. Titanium carbide: synthesis, properties and applications. J. Brill. Eng 2, 1–11.
Mukasyan, A.S., Moskovskikh, D.O., Nepapushev, A.A., Pauls, J.M., Roslyakov, S.I., 2019. Ceramics from self-sustained reactions: recent advances. J. Eur. Ceram. Soc.
Pacheco, M., 2007. Self-sustained High-Temperature Reactions: Initiation, Propagation and Synthesis.
Pratt, T., 2018. Pre-Pregnation of Polymer to Ceramic Resins.
Riley, D.P., Kisi, E.H., Hansen, T.C., 2008. Self-propagating high-temperature synthesis of Ti3SiC2: II. Kinetics of ultra-high-speed reactions from in situ neutron diffraction. J. Am. Ceram. Soc. 91 (10), 3207–3210.
Robertson, I.D., Yourdkhani, M., Centellas, P.J., Aw, J.E., Ivanoff, D.G., Goli, E., Lloyd, E. M., Dean, L.M., Sottos, N.R., Geubelle, P.H., Moore, J.S., White, S.R., 2018. Rapid energy-efficient manufacturing of polymers and composites via frontal polymerization. Nature 557 (7704), 223–227.
Shahzad, K., Deckers, J., Kruth, J.-P., Vleugels, J., 2013. Additive manufacturing of alumina parts by indirect selective laser sintering and post processing. J. Mater. Process. Technol. 213 (9), 1484–1494.
Sohrabi Baba Heidary, D., Lanagan, M., Randall, C.A., 2018. Contrasting energy efficiency in various ceramic sintering processes. J. Eur. Ceram. Soc. 38 (4), 1018–1029.
Sommers, A., Wang, Q., Han, X., T'Joen, C., Park, Y., Jacobi, A., 2010. Ceramics and ceramic matrix composites for heat exchangers in advanced thermal systems—a review. Appl. Therm. Eng. 30 (11), 1277–1291.
Standard ISO18754, I.O.f.S, 2013. 18754, Fine Ceramics (Advanced Ceramics, Advanced Technical Ceramics)-Determination of Density and Apparent Porosity, 8, 15955, 2018.
Stawarczyk, B., Özcan, M., Hallmann, L., Ender, A., Mehl, A., Hämmerlet, C.H., 2013. The effect of zirconia sintering temperature on flexural strength, grain size, and contrast ratio. Clin. Oral Invest. 17, 269–274.
Velasco Gómez, E., Rey Martínez, F.J., Varela Diez, F., Molina Leyva, M.J., Herrero Martín, R., 2005. Description and experimental results of a semi-indirect ceramic evaporative cooler. Int. J. Refrig. 28 (5), 654–662.
Wang, C., Ping, W., Bai, Q., Cui, H., Hensleigh, R., Wang, R., Brozena, A.H., Xu, Z., Dai, J., Pei, Y., Zheng, C., Pastel, G., Gao, J., Wang, X., Wang, H., Zhao, J.-C., Yang, B., Zheng, X., Luo, J., Mo, Y., Dunn, B., Hu, L., 2020. A general method to synthesize and sinter bulk ceramics in seconds. Science 368 (6490), 521.
Wang, X., 2019. Photoinduced Thiol-Ene Click Chemistry Assisted Additive Manufacturing and Freeze Casting of Polymer-Derived Ceramics. Universitätsverlag der TU Berlin.
Wang, X., Schmidt, F., Hanaor, D., Kamm, P.H., Li, S., Gurlo, A., 2019. Additive manufacturing of ceramics from preceramic polymers: a versatile stereolithographic approach assisted by thiol-ene click chemistry. Addit. Manuf. 27, 80–90.
Xu, X., Meteyer, S., Perry, N., Zhao, Y.F., 2015. Energy consumption model of Binder-jetting additive manufacturing processes. Int. J. Prod. Res. 53 (23), 7005–7015.
Yves-Christian, H., Jan, W., Wilhelm, M., Konrad, W., Reinhart, P., 2010. Net shaped high performance oxide ceramic parts by selective laser melting. Phys. Procedia 5, 587–594.
Zhang, Z., Liu, R., Li, W., Liu, Y., Luo, H., Zeng, L., Qiu, J., Wang, S., 2021a. Direct writing of continuous carbon fibers/epoxy thermoset composites with high-strength and low energy-consumption. Addit. Manuf. 47, 102348.
Zhang, Z., Liu, R., Li, W., Liu, Y., Pei, Z., Qiu, J., Wang, S., 2021b. Frontal polymerization-assisted 3D printing of short carbon fibers/dicyclopentadiene composites. J. Manuf. Process. 71, 753–762.